SANDIA REPORT

SAND97-0724 • UC-404
Unlimited Release
Printed April 1997

Nanocavity Effects on Misfit Accommodation in Semiconductors

S. M. Myers, D. M. Follstaedt, S. R. Lee, J. A. Floro, L. R. Dawson, J. L. Reno

Prepared by
Sandia National Laboratories
Albuquerque, New Mexico 87185 and Livermore, California 94550

Sandia is a multiprogram laboratory operated by Sandia Corporation, a Lockheed Martin Company, for the United States Department of Energy under Contract DE-AC04-94AL85000.

Issued by Sandia National Laboratories, operated for the United States Department of Energy by Sandia Corporation.

Available to DOE and DOE contractors from
Office of Scientific and Technical Information
P.O. Box 62
Oak Ridge, TN 37831

Prices available from (615) 576-8401, FTS 626-8401

Available to the public from
National Technical Information Service
U.S. Department of Commerce
5285 Port Royal Rd
Springfield, VA 22161

NTIS price codes
Printed copy: A03
Microfiche copy: A01

SAND97-0724
Unlimited Release
Printed April 1997

Distribution
Category UC-404

Nanocavity Effects on Misfit Accommodation in Semiconductors

S. M. Myers, D. M. Follstaedt, J. A. Floro
Nanostructure and Semiconductor Physics Department

S. R. Lee
Radiation Solid Interactions and Processing Department

L. R. Dawson, J. L. Reno
Semiconductor Material and Device Sciences Department

Sandia National Laboratories
P.O. Box 5800
Albuquerque, NM 87185-1056

Abstract

We report an experimental and theoretical examination of the interaction of dislocations with microscopic cavities in semiconductors and the consequences for strain relaxation in heteroepitaxial structures. Dislocation-mediated relaxation and control of the resulting defect microstructure is central to the exploitation of such heterostructures in devices, and we demonstrate here that the introduction of nanometer-scale voids provides a means of strongly influencing this microstructural evolution. Methods for nanocavity formation using He ion implantation and annealing were developed for Si, SiGe on Si, GaAs, and InGaAs on GaAs. In detailed microstructural studies of SiGe on Si, cavities in the interfacial zone were shown to bind dislocations strongly. This effect reduced the excursion of dislocations into the nearby matrix, although threads into the SiGe overlayer were not eliminated. Interfacial cavities also increased the rate of stress relaxation by more than an order of magnitude as a result of enhanced nucleation of misfit dislocations. Further, in the presence of such cavities, the development of thickness variations in the overlayer during relaxation was suppressed. A theoretical model was developed to describe semiquantitatively the forces on dislocations arising from the combined influences of cavities, misfit strain, and the external surface. Predictions of this model are in accord with microstructural observations.

Acknowledgments

J. C. Barbour provided depth profiling of He by high-energy elastic-recoil detection. The ion implantations were carried out by G. A. Petersen. M. P. Moran prepared specimens for transmission electron microscopy. The authors benefited from several discussions with B. W. Dodson concerning the interactions of dislocations with voids. This work was supported by the U. S. Department of Energy under Contract DE-AC04-94AL85000, and was carried out under the auspices of the Laboratory Directed R&D Department of Sandia National Laboratories.

Contents

Figures

Nanocavity Effects on Misfit Accommodation in Semiconductors

Introduction

In layered devices formed by heteroepitaxial growth of Si-Ge or compound-semiconductor alloys on substrates with a different lattice parameter, structural relaxation of the overlayer occurs through the formation of interfacial misfit dislocations [1-3]. It is desirable to maximize the degree of relaxation during this process, and it is critical to limit the propagation of dislocations into the device-containing region of the overlayer. Indeed, the latter constraint has limited the range of epitaxial structures available for advanced, bandgap-engineered materials [4,5].

In the present investigation, we examined the influence of microscopic cavities on the behavior of dislocations in semiconductor heteroepitaxial structures. This study was motivated by the possibility that an anticipated strong attraction between the dislocations and open volumes could be exploited to control dislocation movement. Formation of cavities in Si and Ge was previously achieved by ion-implanting He and then annealing to induce diffusion of the gas from the specimen, leaving a layer of nanometer-size voids [6-8]. In the present study, we employed He implantation to form thin interfacial cavity layers in SiGe-on-Si heterostructures. Moreover, by using a variation of the method, we successfully addressed the greater challenge of forming stable cavities in GaAs and in InGaAs-on-GaAs. Observations of the evolution of dislocation and cavity microstructures in He-implanted Si, Ge, and SiGe-on-Si revealed a variety of effects of cavity-dislocation binding, and these were interpreted using theoretical models. Our results also indicate that interfacial cavities strongly promote nucleation of misfit dislocations. The consequences of these phenomena for strain relaxation in heterostructures and for the resultant defect microstructure were examined in the model SiGe-on-Si system, and wider implications were drawn.

Cavity Formation

Figure 1 shows a representative He implantation profile in Si, calculated using the Monte-Carlo range code TRIM [9]. When Si is implanted at room temperature under these conditions and then annealed for 30 minutes at 700°C, causing diffusion of most of the He from the specimen [6,10], a layer of cavities results, as seen in the cross-section transmission electron microscopy (TEM) image of Fig. 2a. Such cavities are highly stable in Si: further annealing at temperatures extending above 1100°C produces coalescence and enlargement, and diminishes other implantation-related defects including dislocations, but does not disrupt the overall integrity and localization of the void-containing layer.

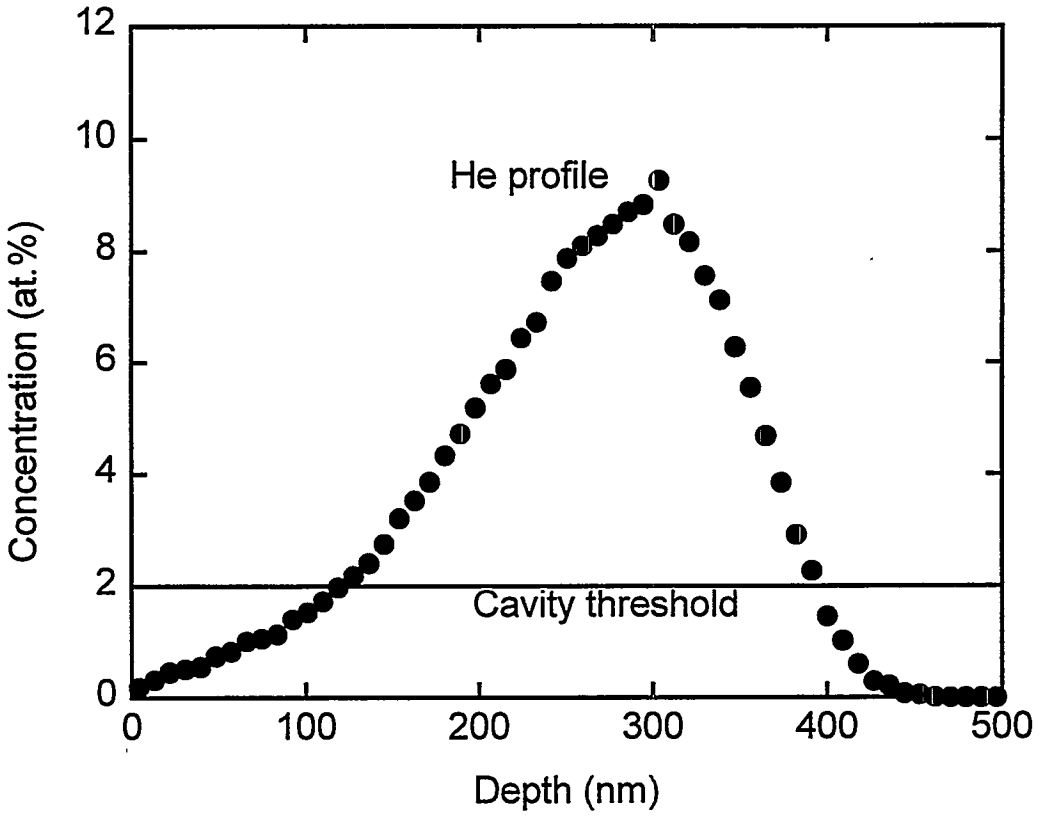

Fig. 1. Concentration-versus-depth profile of ion-implanted He in Si calculated using TRIM. The calculation treated an implantation of 1×10^{17} He/cm^2 at 30 keV, and the depth scale was multiplied by 0.88 to produce agreement with the TEM image in Fig. 2a.

When cavities are used as dislocation traps in the interfacial region of heterostructures, it is desirable to restrict the depth distribution more narrowly than in Fig. 2a. This can be achieved by exploiting the fact that the threshold He concentration for cavity nucleation is appreciable, being about 2 at.% in Si [8]. As a result, implanting smaller He concentrations reduces the width of the layer. The concept is illustrated by scaling the He implantation profile of Fig. 1 progressively downward in concentration, corresponding to smaller implantation doses, while defining the width of the cavity layer as the distance between the intercepts with a horizontal line at 2 at.%. The predicted narrowing is confirmed in experiments, as illustrated by the cross-section TEM image in Fig. 2b.

The depth distribution of interfacial cavities can be tailored to an even greater degree by implanting the He at lower energies during a temporary interruption of the growth of the epitaxial overlayer. In order to implement this procedure, we incorporated an ion gun into the chamber used for molecular-beam epitaxy. An example of the microstructure obtained is shown in Fig. 3.

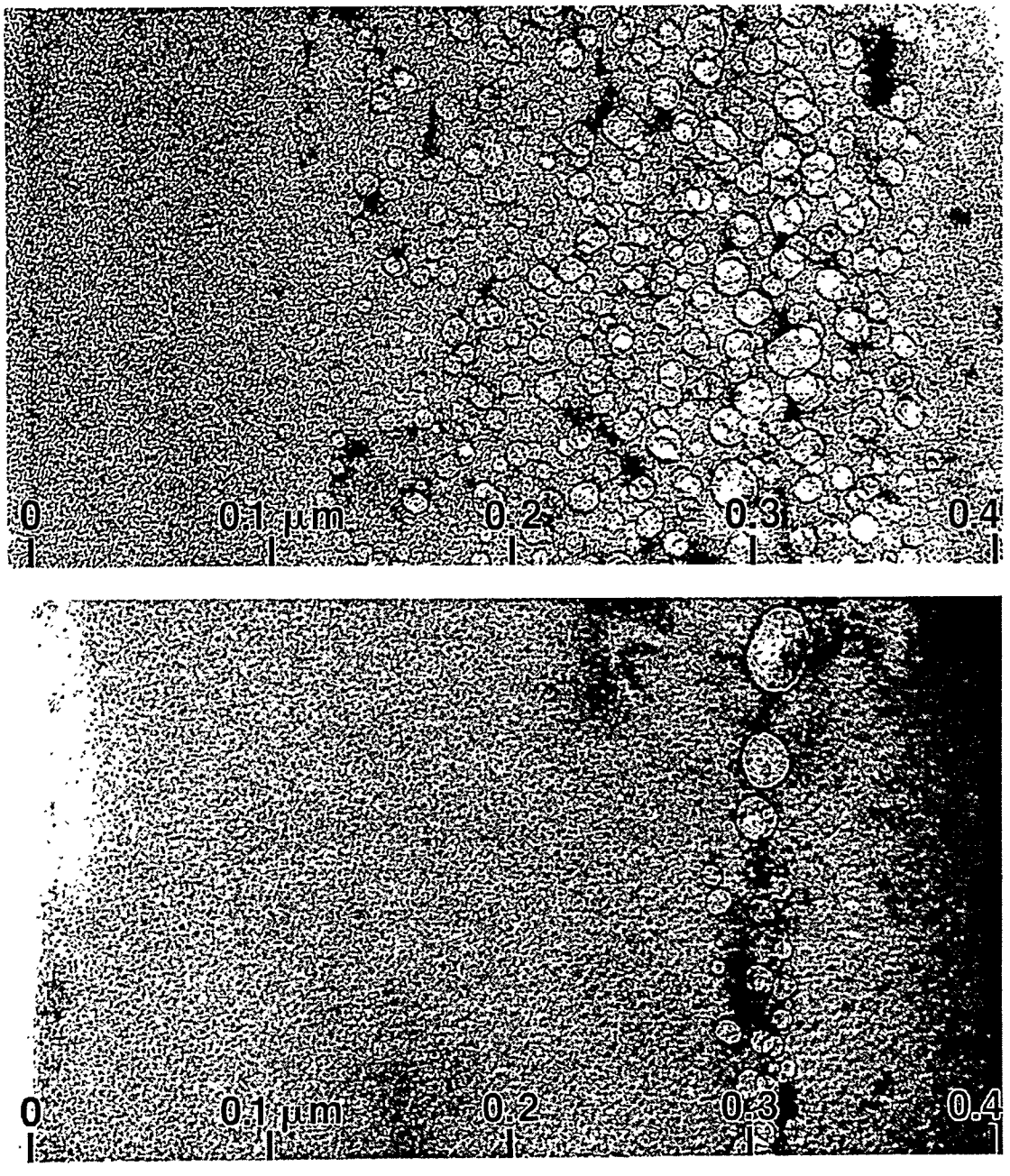

Fig. 2. Cross-section TEM images of cavities in Si implanted with He and annealed. The He was implanted at 30 keV to a dose of (a) 1×10^{17} cm^{-2} or (b) 2×10^{16} cm^{-2}, and the specimen was subsequently annealed for 30 minutes at 700°C. The cavity open volumes were made visible by operating the electron microscope at slight underfocus.

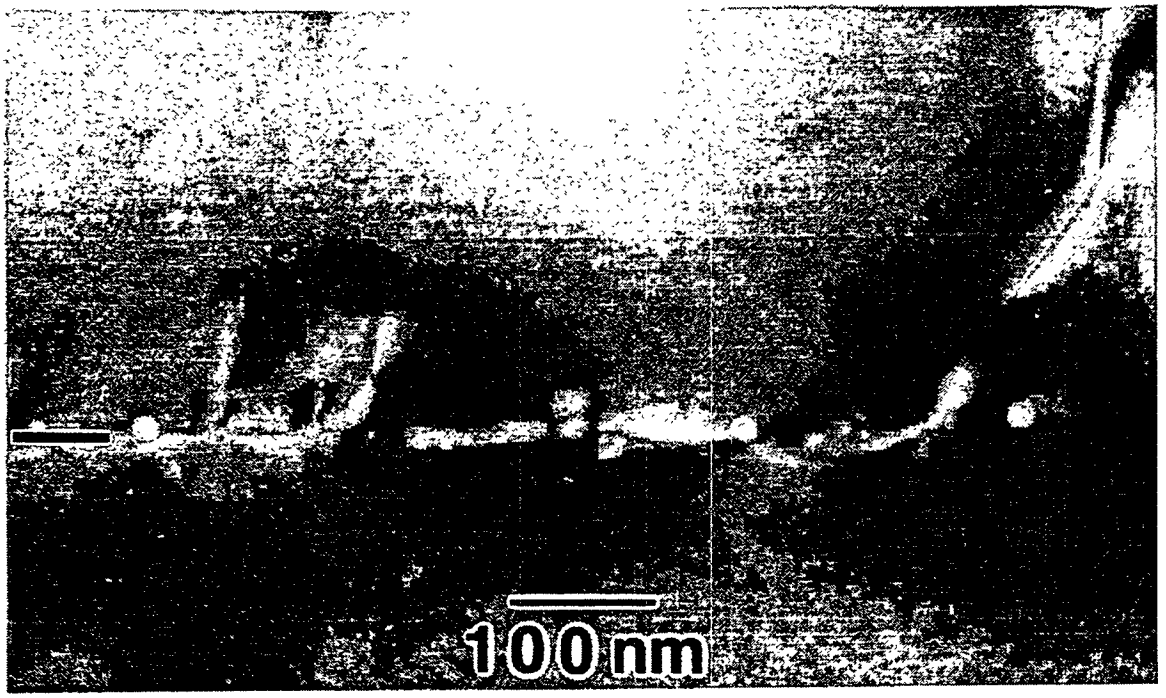

Fig. 3. Interfacial cavities in SiGe on Si implanted with He during growth. Growth of $Si_{83}Ge_{17}$ by molecular-beam epitaxy at 550°C was interrupted at a thickness of 50 nm for cavity formation and then continued to a total thickness of 275 nm. The cavities were formed by implanting 2×10^{16} He/cm^2 at 4.5 keV and then annealing for 30 minutes at 700°C. The position of the interface is indicated by the bar at the left margin.

The formation of stable cavities in GaAs and InGaAs-on-GaAs proved more challenging. When these materials are implanted with He at room temperature to concentrations above the threshold for bubble formation and then heated under vacuum to a temperature of 250°C or higher, fracture occurs within the bubble-containing region prior to He release, leading to exfoliation of the overlayer. In initial efforts to avoid this effect, the He was implanted at elevated temperatures with the objective of promoting simultaneous, thermally activated lattice recovery; however, the microstructural instability during post-implantation annealing persisted for implantation temperatures up to 250°C, and, when the injection was carried out at 300 or 400°C, the He escaped from the specimen during the implantation process without the formation of cavities. Since the latter temperatures lie above important defect-recovery stages for GaAs, we inferred that the mobile He escaped before encountering defect traps of sufficient strength to accumulate multiple atoms and thereby nucleate bubbles. This led to the final and successful procedure: first, a low dose of Ar atoms was implanted into the intended cavity layer while the sample was held at 400°C, in order that these larger and less mobile atoms would produce persistent nuclei for the subsequent accumulation of He; the He was then implanted at the same temperature, giving rise to a dense array of bubbles; finally, more extended annealing at 400°C induced diffusion of the He from the material, as shown by high-energy elastic-recoil detection, leaving the

Fig. 4. Cavities in InGaAs on GaAs. The 330-nm $In_{10}Ga_{90}As$ layer was grown by molecular-beam epitaxy at 530°C. Cavities were subsequently formed by implanting 1×10^{16} Ar/cm^2 at 360 keV and then 5×10^{16} He/cm^2 at 50 keV, both at a temperature of 400°C. The overlayer-substrate interface is at a depth of 0.33 μm.

evacuated cavities. A representative microstructure resulting from this sequence is seen in the cross-section TEM image of Fig. 4.

Theoretical Consideration of Dislocation-Cavity Interactions

Cavities are expected to attract dislocations as a result of two effects: first, the strain energy associated with the elastic distortion field about the dislocation disappears within the open volume and is also reduced in the immediate vicinity of the cavity by relaxation; additionally, when the dislocation core intersects the cavity, the effective core energy is greatly reduced. In order to estimate the strength of this interaction, we developed an approximate theoretical treatment of the energies involved. Our approach was guided by a full, analytical treatment of the influence of cavities on strain fields in three relatively simple

geometries: 1) a spherical cavity centered within a radially distorted spherical solid, 2) a long cylindrical cavity along the axis of a long cylindrical solid that is radially distorted, and 3) a similar cylindrical configuration with an externally imposed contortion that, in the absence of the cavity, would produce uniform planar shear with the cylindrical axis lying in the plane of the shear. The equations governing the strain displacement field and the means of their solution in such high-symmetry situations have been discussed elsewhere [11,12].

A key finding from the above case studies is that the increase in total strain energy, ΔW, caused by moving a cavity from a strained region into an unstrained zone is comparable to the algebraic sum of two more easily calculated quantities: the post-transfer strain energy of the material occupying the original cavity volume, ΔW_V, and the negative of the work, ΔW_S, that would be done by the lattice strain against the surface tension of the cavity wall if that lattice strain were unchanged by the presence of the cavity. The ratio $\Delta W/(\Delta W_V - \Delta W_S)$ is not strongly dependent upon the strain environment of the cavity, the value being ~2 for the cases that were solved fully. (The departure from unity arises from the contortion of the non-rigid cavity volume and surrounding material.) Hence, in modeling more complicated conditions where an exact solution is not feasible, we estimated the strain energy by first calculating $\Delta W_V - \Delta W_S$ by numerical volume integration and then applying a correction factor of ×2. In accord with well established practice [3,11], the core energy of the dislocations was artificially incorporated into the elastic-strain integral by extending this integral inward to a small radius of b/4, where b is the length of the Burgers vector.

The characteristics of the dislocation-cavity interaction are illustrated in Fig. 5, which shows binding energy as a function of the distance, R, of a screw dislocation from the center of a spherical cavity of 10-nm radius within Si, as calculated using the above approximate theoretical approach. (There is no influence of cavity surface tension here, $\Delta W_S = 0$. Within the approximations of our model, the surface tension does not couple to the purely shear strain induced by the screw dislocation.) The binding energy is seen to be large, reaching about 800 eV when the dislocation passes through the center of the cavity. The attraction is short-range, however, with binding energy varying as R^{-2} and force as R^{-3} for large R. The interaction of an edge dislocation is more complicated but shares these two characteristics.

The combined influences of a dense cavity layer and the external surface on a dislocation are exemplified in Fig. 6, where the calculated strain energy associated with a screw dislocation in Si parallel to the surface is plotted as a function of the distance, X, of the dislocation from the surface. The assumed cavity volume fraction as a function of depth was chosen to conform to the TEM micrograph of Fig. 2a and is also shown. The cavities were treated mathematically as a continuous distribution of open volume, and the effect of the external surface was introduced through a mirror-image dislocation strain field [11]. This figure exhibits the relatively large size of the surface attraction, and also its long range, with the effective force on the dislocation varying as X^{-1}. There is a depth interval of metastability for dislocations within the cavity layer, but a dislocation-free zone is predicted to occur between the cavities and the surface. Both features are evident in Fig. 7, where the microstructure of Fig. 2a is imaged with the dislocation strain fields in strong contrast.

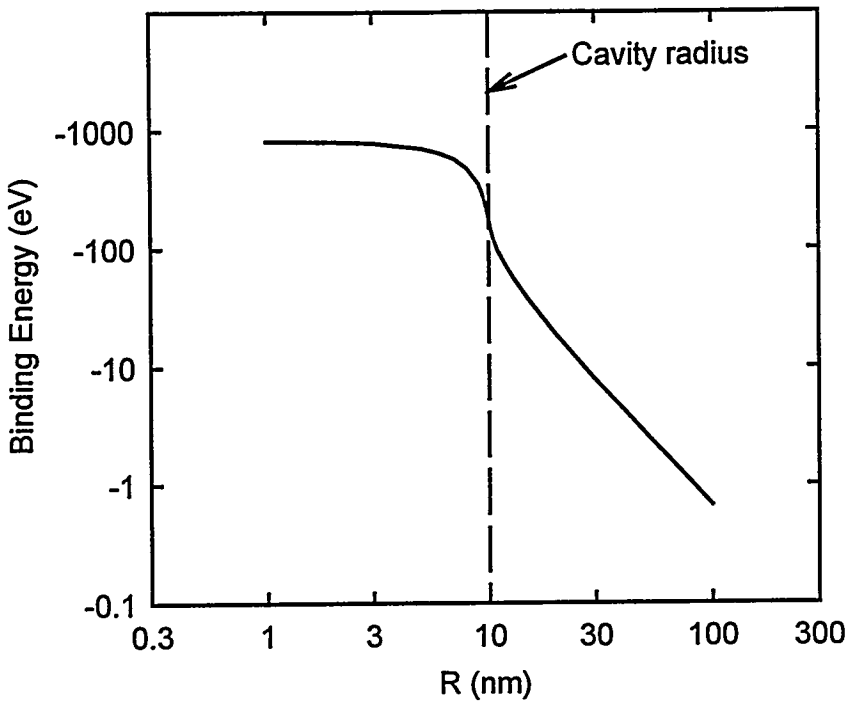

Fig. 5. Calculated binding energy between a cavity and a screw dislocation in Si.

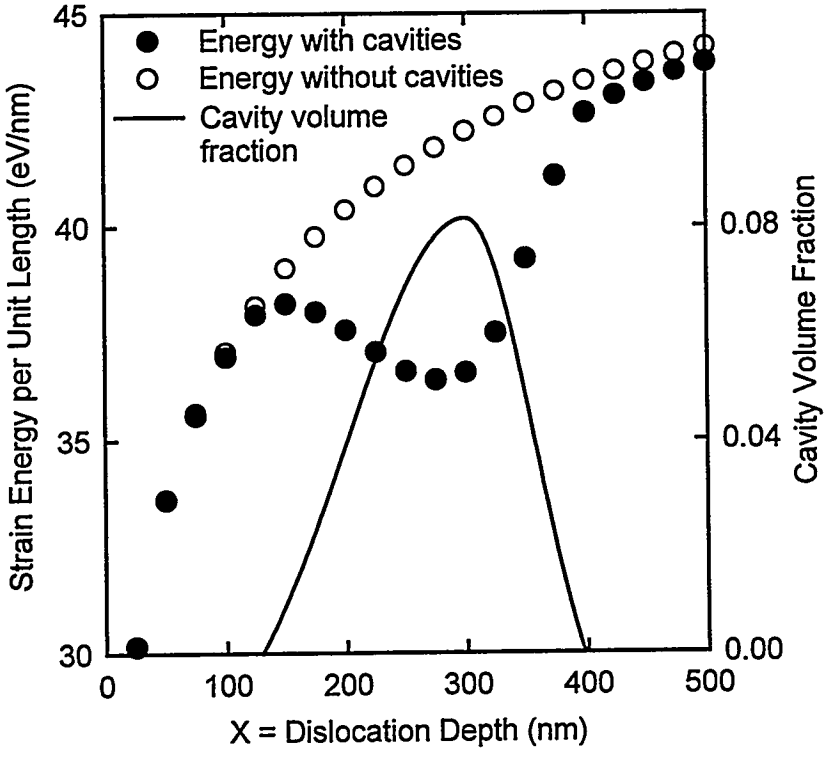

Fig. 6. Calculated strain energy of a screw dislocation in the vicinity of the surface and a cavity layer similar to that in Fig. 2a.

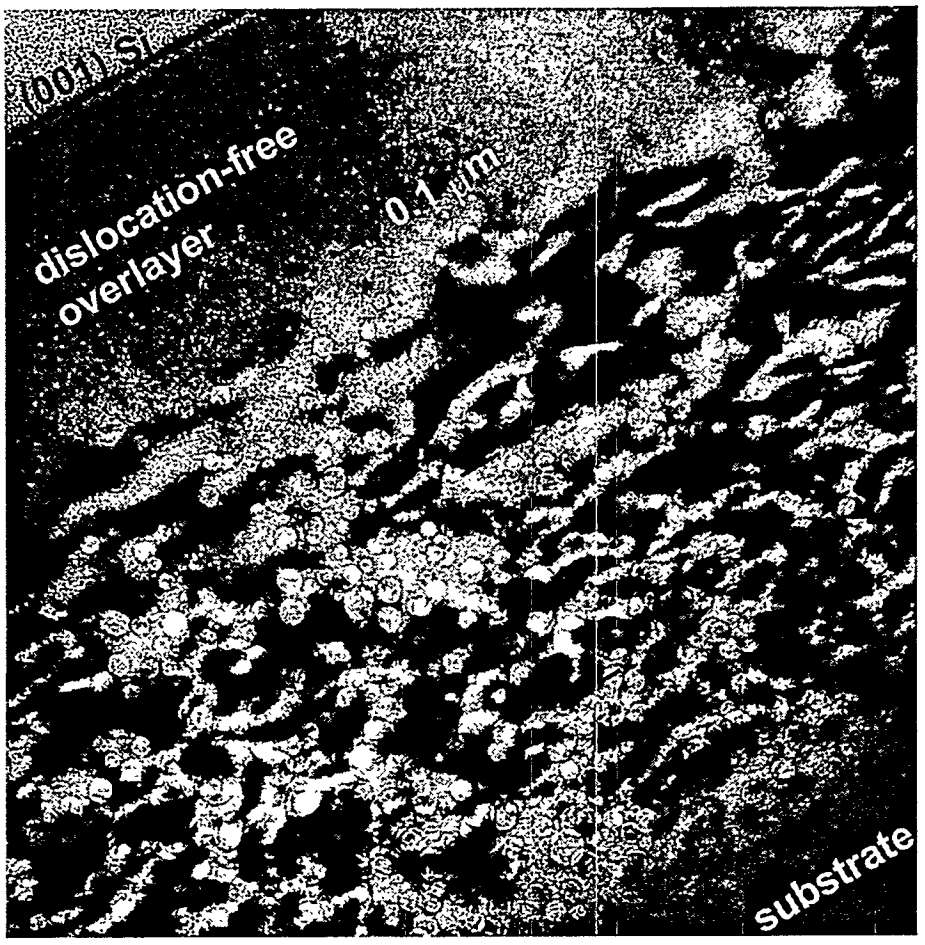

Fig. 7. Dislocations localized within a cavity layer in Si. Helium was implanted at 30 keV to a dose of 1×10^{17} cm^{-2}, and the specimen was subsequently vacuum-annealed for 30 minutes at 700°C. The strain fields of the dislocations are in dark contrast.

Cavity-Dislocation Microstructures and Strain Relaxation in Si-Ge

Ion implantation of He and the resultant formation of cavities produce dislocations in Si and Ge even in the absence of pre-existing misfit strain, and TEM reveals a clear affinity of these dislocations for cavities. In Fig. 7, this affinity is evidenced by the overall localization of dislocations within the cavity layer in Si. Figure 8 shows an enlarged image obtained after a similar cavity-formation treatment of Ge. Here, the larger size and smaller number of cavities allow a more detailed examination, and the intersection of dislocations with cavities is apparent. The microstructural characteristics in these two figures are consistent with the strong binding of dislocations to cavities seen in Fig. 5 and with the predicted positional metastability within the cavity layer exhibited in Fig. 6.

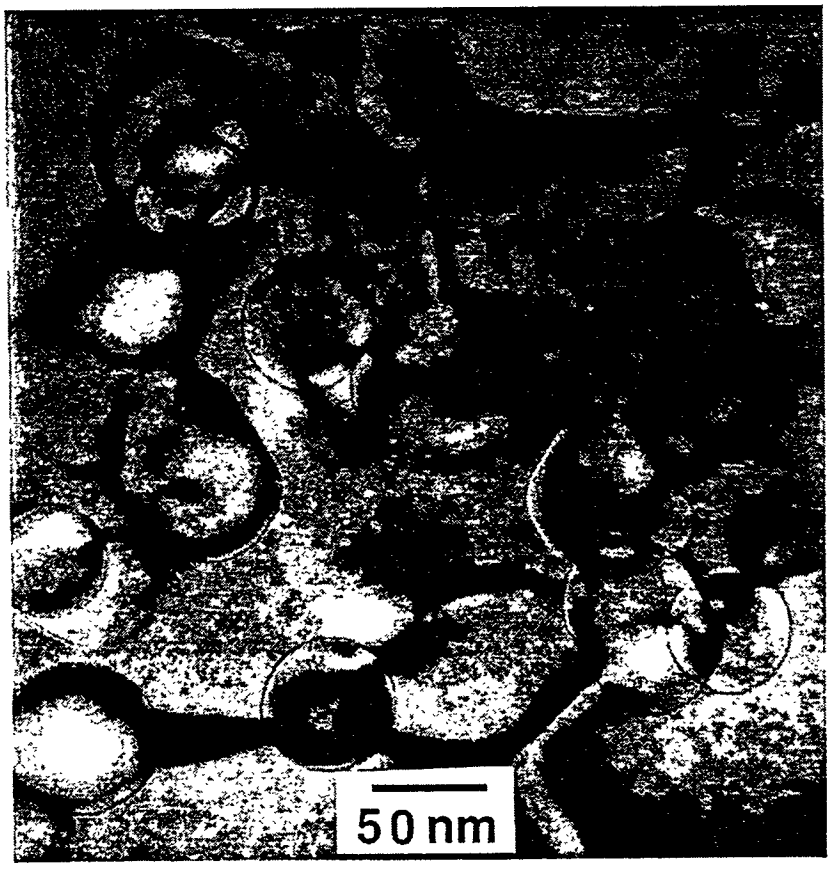

Fig. 8. Cavities and dislocations in Ge. Helium was implanted at 50 keV to a dose of 1×10^{17} cm^{-2}, and the specimen was subsequently vacuum-annealed for 1 hour at 700°C. The strain fields of the dislocations are in dark contrast.

The interaction of misfit dislocations with interfacial cavities in relaxed SiGe on Si is illustrated in Fig. 9, which shows cross-section and plan-view TEM images in which both the cavities and the dislocation strain fields are in contrast. In this case, the He was injected into the interfacial region of a fully grown and initially unrelaxed heterostructure, which then underwent relaxation and cavity formation during annealing at 900°C. In contrast to the regular, crossed arrays of nearly straight misfit dislocations that are observed in the absence of cavities, the misfits here are seen to undergo substantial lateral excursions in order to intersect the cavities and thereby reduce strain and core energies. Similar behavior was observed in a heterostructure whose SiGe growth was interrupted at a thickness of 50 nm for *in-situ* He implantation at a lower energy, as seen in Fig. 10.

Because of the relatively short range of the cavity-dislocation binding, the large influence on misfit dislocations seen in Figs. 9 and 10 requires that the depth of the cavity layer coincide with that of the interface. The result of noncoincidence is seen in Fig. 11, where the cavities lie several tens of nanometers beneath the interface. The plan-view image in Fig. 11b shows that, while non-misfit dislocations within the cavity layer are bound to the cavities, the misfit array itself is largely unaffected.

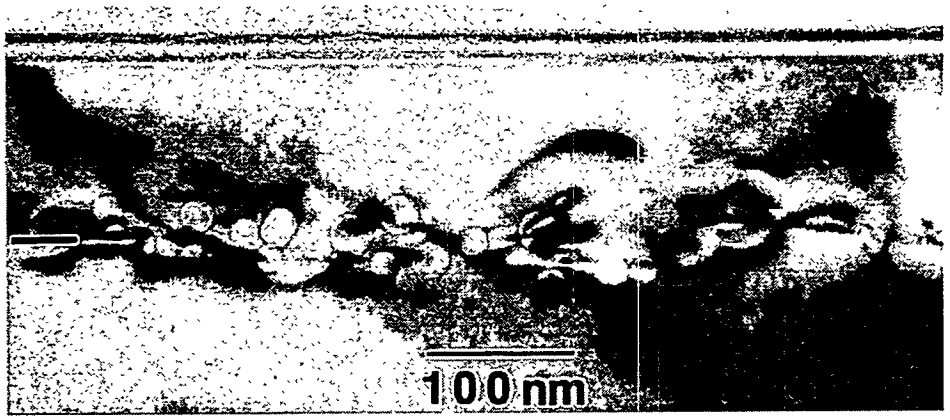

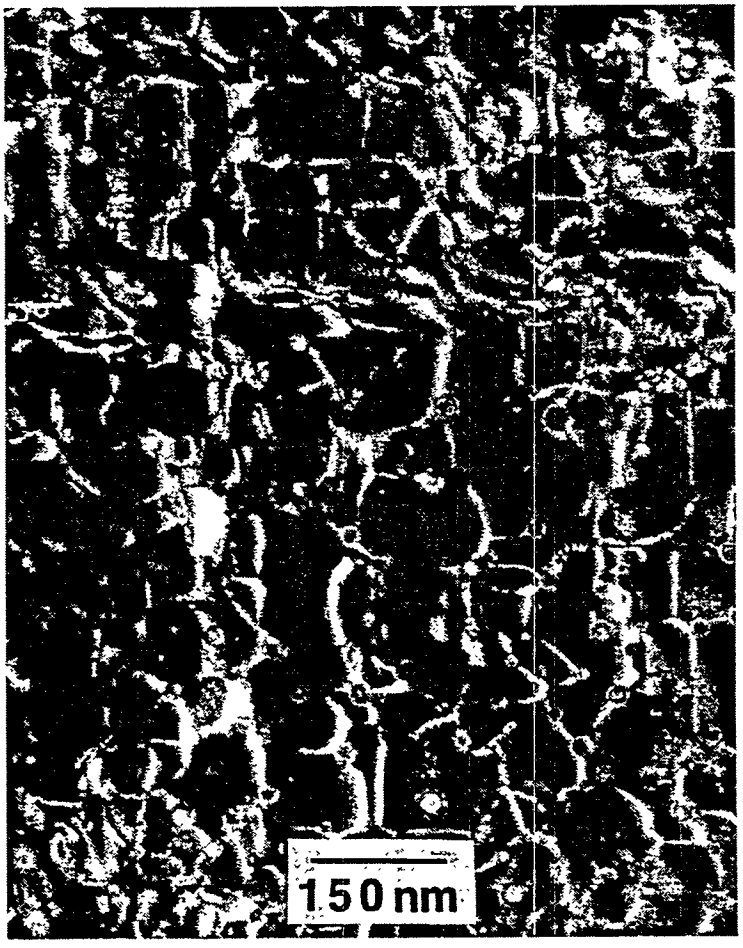

Fig. 9. Interfacial cavities and dislocations in SiGe on Si. The 140-nm $Si_{86}Ge_{14}$ alloy was grown by chemical vapor deposition and was initially fully strained. The cavities were introduced by implanting 1.7×10^{16} He/cm^2 at 15 keV and an incident angle of 30° from the normal and then vacuum annealing for 1 hour at 900°C, with stress relaxation occurring during the anneal. (a) Bright-field image in cross-section. (b) Dark-field, weak-beam image in plan-view.

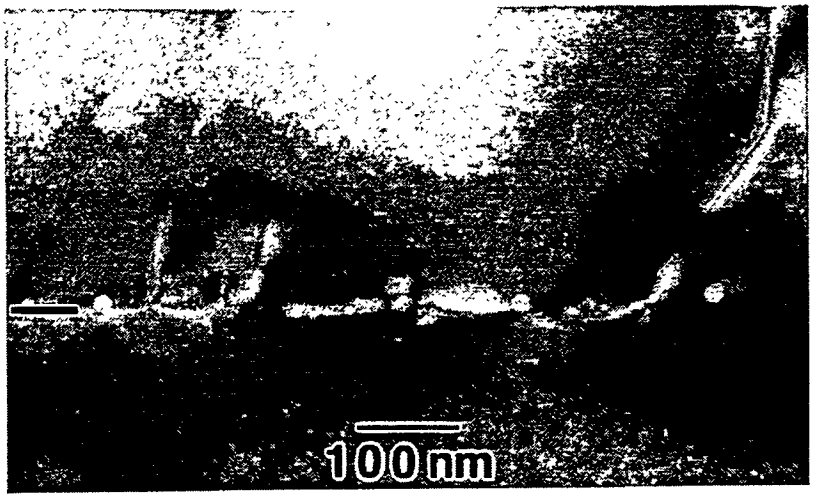

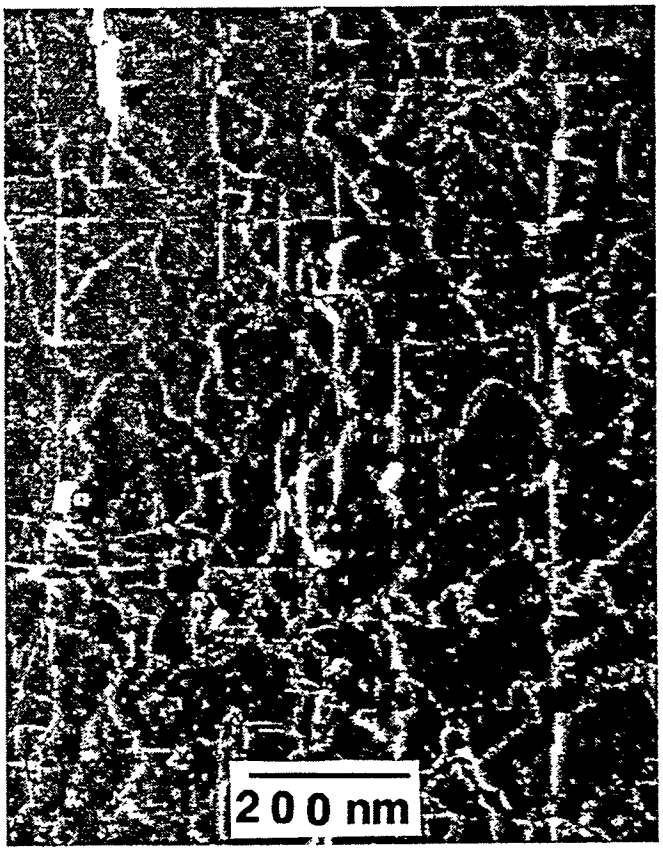

Fig. 10. Interfacial cavities and dislocations in SiGe on Si implanted with He during growth. Growth of $Si_{83}Ge_{17}$ by molecular-beam epitaxy at 550°C was interrupted at a thickness of 50 nm for cavity formation and then continued to a total thickness of 275 nm. The cavity formation was accomplished by implanting 2×10^{16} He/cm^2 at 4.5 keV and then annealing for 30 minutes at 700°C. (a) Bright-field image in cross-section. (b) Dark-field, weak-beam image in plan-view.

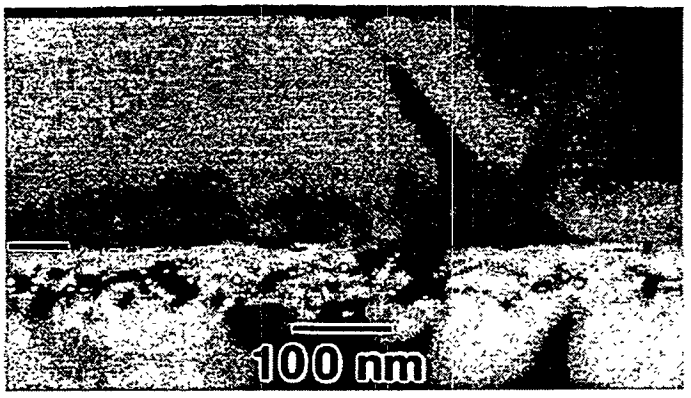

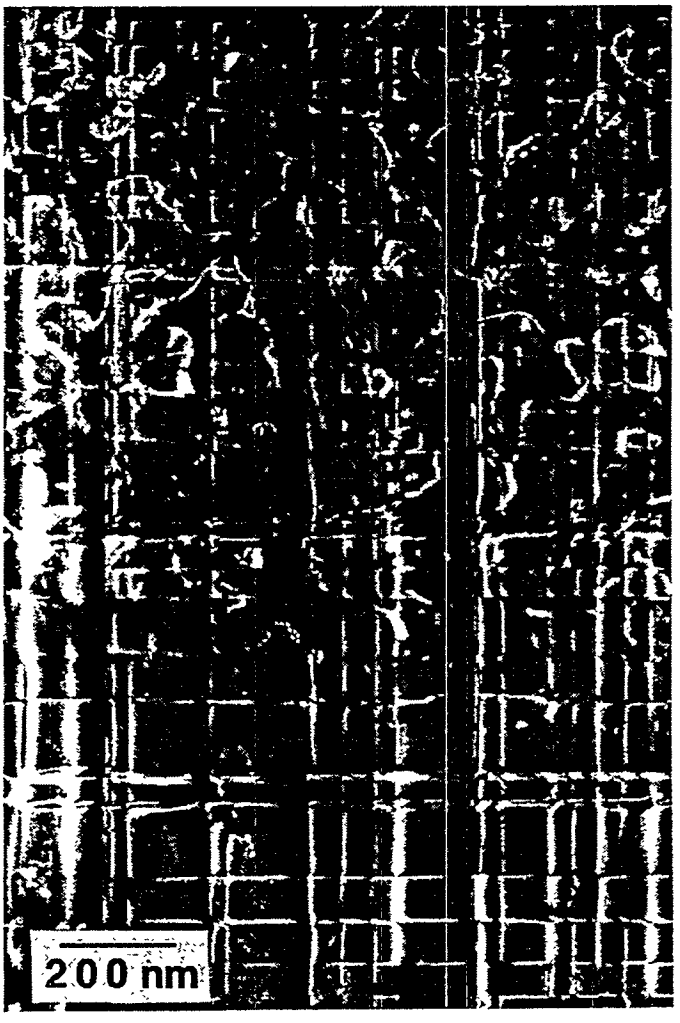

Fig. 11. Microstructure of SiGe on Si with He implanted below the interface before SiGe growth. Sample treatment was otherwise the same as for Fig. 10. (a) Bright-field image in cross-section. (b) Dark-field image in plan-view. Specimen thickness increases from bottom to top in the plan-view image, so that the lower portion exhibits only the interface with its misfit dislocations, while the upper portion includes the cavity layer.

The introduction of an interfacial cavity layer substantially accelerates the relaxation of misfit strain in SiGe-on-Si heterostructures during annealing. This effect is seen in Table 1, which compares the fractional relaxation of initially fully strained SiGe on Si with and without an interfacial cavity layer after three vacuum heat treatments. The overlayer was grown by chemical vapor deposition to a thickness of 140 nm, and its composition was $Si_{86}Ge_{14}$, implying a lattice mismatch of approximately 0.5 %; the conditions of He implantation were the same as those leading to the microstructure of Fig. 9. In the case of the one-hour anneal at 900°C, the extent of relaxation is at least fifty times greater when cavities are present. Two contributions to this difference are conceivable: 1) nucleation of misfit dislocations at the cavities and related defects, and 2) more rapid propagation of the misfits as a result of their reduced formation energy in a region containing cavities. The size of the latter effect can be estimated by calculating the opposing driving forces due to the overlayer-misfit strain and the energy expenditure required for formation of misfit dislocations [3]; under the conditions in question, this yields a relatively small increase of $\lesssim$10% in the relaxation rate. Hence, we conclude that the observed large increase resulted predominantly from enhanced nucleation.

Table 1. Relaxation of SiGe on Si during annealing with and without cavities.

Anneal	Relaxation - no cavities	Relaxation - with cavities
1 hour at 900°C	<1%	54%
1 hour at 1000°C	20-69%	81%
4 hours at 1000°C	43%	79%

The relaxed microstructure of the SiGe-on-Si heterostructure is influenced by interfacial cavities in several ways. First, as seen from the comparison of cross-section TEM images in Fig. 12, dislocations in the vicinity of the interface are confined more closely to the interface when cavities are present. Second, residual threading dislocations in the cavity-containing material usually cross directly to the surface, rather than having extended segments parallel to the surface as is observed in the absence of cavities. The areal density of the threads is not significantly changed by the cavities, however, being approximately 7×10^9 cm^{-2} for the conditions of Fig. 12. Finally, relaxation of the heterostructure without cavities gives rise to thickness variations of ~10 nm, whereas no such undulations were found when the cavities were present. These effects are ascribed to the attraction of dislocations to the cavity layer and to the more prompt relaxation due to easier nucleation of dislocations.

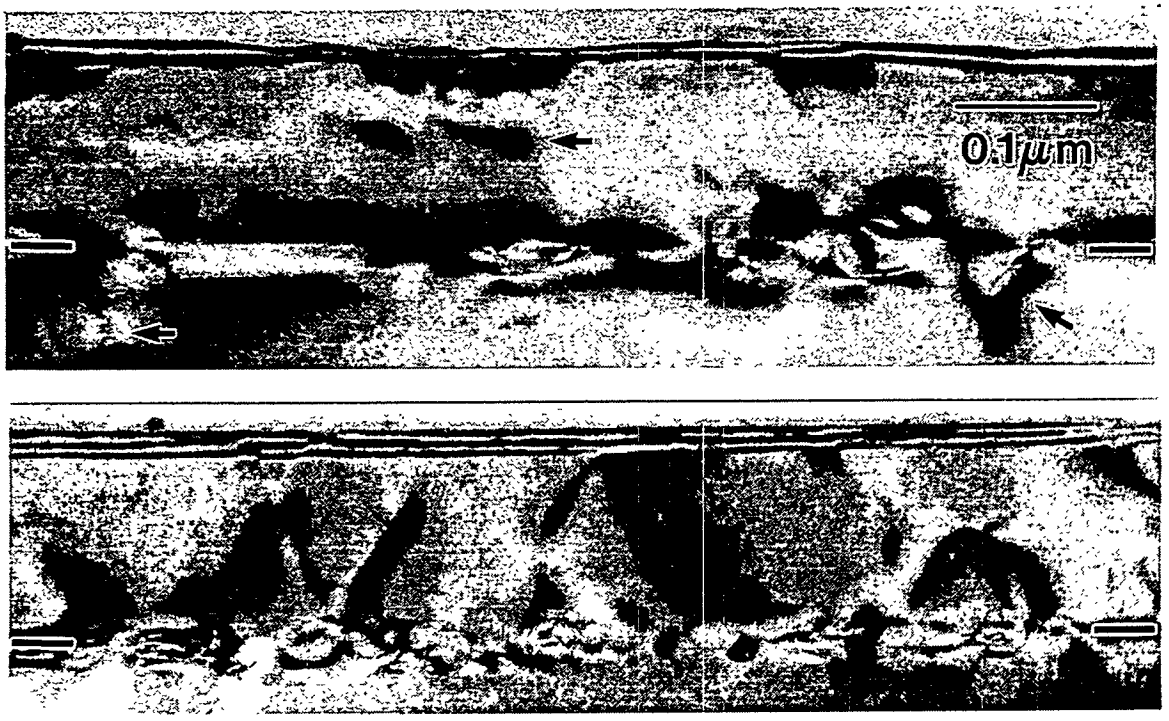

Fig. 12. Dislocation microstructure in relaxed SiGe on Si with and without cavities. (a) No He implantation. (b) With He implantation. The starting material and the He-implantation conditions were the same as for Fig. 9. The specimens were finally vacuum-annealed for 1 hour at 1000°C. The arrows in (a) point to dislocations extending into the Si substrate and lying parallel to the surface within the SiGe layer.

Discussion and Conclusions

This work demonstrated that a narrow band of cavities is readily introduced into the interfacial region of SiGe-on-Si heterostructures by means of He ion implantation and annealing, either during growth or afterward. These cavities strongly bind dislocations, as theoretically predicted and experimentally observed. The He-implanted layer also serves as an effective nucleation source for misfit dislocations, thereby increasing the rate of stress relaxation by more than an order of magnitude. The relaxed microstructure is improved by the cavities, which lead to better confinement of dislocations at the interface, less lateral extension of residual threading dislocations, and less development of overlayer thickness variations during the relaxation process. In the present studies, however, the areal density of threads was not found to be reduced by the cavities.

In this initial investigation, we did not examine the interplay of cavities with compositionally graded buffer layers, which have been shown to reduce threading-dislocation densities significantly [13,14]. The combined influence of two such potent perturbations of dislocation behavior would appear to warrant study in the future. The present experiments were also limited to SiGe-on-Si heterostructures that were laterally uniform over millimeter

distances, so that strain relaxation without macroscopic movement of material required the propagation of threading dislocations or other shear-accommodating imperfections through the overlayer. As a result, the observation of residual threads within the overlayer, with or without cavities, is not surprising. This consideration suggests that cavity effects should also be investigated in two types of structure not examined here: 1) lateral networks of cavities designed to trap the threads within restricted zones; and 2) mesas with lateral dimensions in the micrometer range, where cavity-assisted thread propagation to the edge, and perhaps even cavity-related plastic compliance without any passage of imperfections through the overlayer, are conceivable.

Our studies showed that stable cavity layers can also be introduced into GaAs and InGaAs on GaAs, although more elaborate procedures are required to overcome the susceptibility of these materials to fracture during heating after implantation. The effects of the cavities on dislocation behavior and on strain relaxation were not examined sufficiently to permit definitive conclusions, but the occurrence of processes paralleling those found in SiGe on Si is plausible.

The overall conclusions from this work are that cavities strongly influence dislocation behavior and strain relaxation in semiconductor heteroepitaxial structures and that these effects show promise for exploitation in devices. Realization of the potential benefits in enhanced relaxation and defect suppression will require further research, including the areas of study enumerated above.

Elements of this multifaceted work have been published [15-18], and it is intended that all aspects will ultimately appear in the literature.

References

[1] *Strained-Layer Superlattices: Materials Science and Technology*, T. P. Pearsall, ed. Academic Press, New York, 1991.

[2] R. Hull and J. C. Bean, Misfit Dislocations in Lattice-Mismatched Epitaxial Films, in Crit. Rev. in *Solid State and Mater. Sci.*, vol. 17, pp. 507-546, 1992.

[3] J. Y. Tsao, *Materials Fundamentals of Molecular Beam Epitaxy*, pp. 151-197. Academic Press, San Diego, 1993.

[4] J. C. Bean, Silicon-Based Semiconductor Heterostructures: Column IV Bandgap Engineering, in *Proc. IEEE*, vol. 80, pp. 571-587, 1992.

[5] *High-Speed Heterostructure Devices*, R. A. Kiehl and T. C. L. G. Sollner, ed. Academic Press, New York, 1994.

[6] C. C. Griffioen, J. H. Evans, P. C. De Jong, and A. Van Veen, Helium Desorption/Permeation from Bubbles in Silicon: A Novel Method of Void Production, in *Nucl. Instrum. Methods B*, vol. 27, pp. 417-420, 1987.

[7] S. M. Myers, H. J. Stein, and D. M. Follstaedt, Hydrogen Interactions with Cavities in Helium-Implanted Germanium, in *Phys. Rev. B*, vol. 51, pp. 9742-9751, 1995.

[8] D. M. Follstaedt, S. M. Myers, G. A. Petersen, and J. W. Medernach, Cavity Formation and Impurity Gettering in He-Implanted Si, in *J. Electr. Mater.*, vol. 25, pp. 151-163, 1996.

[9] J. F. Ziegler, J. P. Biersack, and U. Littmark, *The Stopping and Range of Ions in Solids*. Pergamon Press, New York, 1985.

[10] A. Van Wieringen and N. Warmoltz, The Permeation of Hydrogen and Helium in Single Crystal Silicon and Germanium at Elevated Temperatures, in *Physica*, vol. 22, pp. 849-865, 1956.

[11] J. P. Hirth and J. Lothe, *Theory of Dislocations*, Second Edition. Krieger Publishing, Malabar, Florida, 1992.

[12] L. D. Landau and E. M. Lifshitz, *Theory of Elasticity*, Third Edition. Butterworth-Heinemann, Oxford, 1986.

[13] E. A. Fitzgerald, Y. H. Xie, D. Monroe, G. P. Watson, J. M. Kuo, and P. J. Silverman, Defect Control in Relaxed, Graded GeSi/Si, in *Mater. Sci. Forum*, vols. 143-147, pp. 471-482, 1994.

[14] P. M. Mooney, F. K. LeGoues, and J. O. Chu, Origin of Mosaic Structure in Relaxed $Si_{1-x}Ge_x$ Layers, in *Mater. Sci. Forum*, vols. 143-147, pp. 483-488, 1994.

[15] D. M. Follstaedt, S. M. Myers, G. A. Petersen, and J. C. Barbour, Cavity Nucleation and Evolution in He-Implanted Si and GaAs, in *Mat. Res. Soc. Symp. Proc.*, vol. 396, pp. 801-806, 1996.

[16] D. M. Follstaedt, S. M. Myers and S. R. Lee, Cavity-Dislocation Interactions in Si-Ge and Implications for Heterostructure Relaxation, in *Appl. Phys. Lett.*, vol. 69, pp. 2059-2061, 1996.

[17] D. M. Follstaedt, S. M. Myers, J. A. Floro, and S. R. Lee, Interaction of Cavities with Misfit Dislocations in SiGe/Si Heterostructures, in *Nucl. Instrum. Methods B*, in press, 1997.

[18] D. M. Follstaedt, S. M. Myers, and S. R. Lee, Interaction of Cavities and Dislocations in Si-Ge, in *Mat. Res. Soc. Symp. Proc.*, in press, 1997.

DISTRIBUTION:

1	MS-0601	L. R. Dawson, 1113
1	MS-0601	J. S. Nelson, 1113
1	MS-0601	J. L. Reno, 1113
1	MS-1056	B. L. Doyle, 1111
1	MS-1056	D. M. Follstaedt, 1112
1	MS-1056	S. R. Lee, 1111
2	MS-1056	S. M. Myers, 1112
1	MS-1415	J. A. Floro, 1112
1	MS-1415	W. B. Gauster, 1112
1	MS-0188	LDRD Office, 4523
2	MS-0619	Review & Approval Desk, 12690 (for DOE/OSTI)
5	MS-0899	Technical Library, 4414
1	MS-9018	Central Technical Files, 8940-2